

**Study of Initial Vorticity Forcing for Block Onset by a 4-Dimensional  
Variational Approach**

Fangli Qiao\*

*First Institute of Oceanography, SOA, Qingdao, China*

S. Zhang

*Geophysical Fluid Dynamics Laboratory, Princeton University*

*Princeton, NJ 08542, USA*

Xunqiang Yin

*First Institute of Oceanography, SOA, Qingdao, China*

(Final version: January 2004)

(submitted to **Adv. Atmos. Sci.**)

\* *Corresponding author address:* Fangli Qiao, No. 6, Xianxia Ling Rd., High-Tech Park, Qingdao, 266061. Email: flqiao@21cn.com Tel: (532)889-0055

## ABSTRACT

With the aid of a global barotropic model, the role of the interaction of the synoptic-scale disturbance and the planetary flow in block onset is examined by a 4-dimensional variational approach. A cost function is defined to measure the squared errors of the forecasted streamfunctions during block onset period (day 4 and day 5 in this study) over a selected blocking domain. The sensitivity of block onset with respect to the initial synoptic-scale disturbance is studied by examining the gradient of the defined cost function with respect to the initial (during the first 24-hour) vorticity forcing, which is evaluated by the adjoint integration. Furthermore, the calculated cost function and gradient is connected with the limited memory quasi-Newton optimization algorithm for solving the optimal initial vorticity forcing for block onset.

For two studied cases of block onset (northern Atlantic and northern Pacific) introducing the optimal initial vorticity forcing the nonlinear barotropic advection process mostly reconstructs these blocking onset processes. These results show that the formation of blocking can be correctly described by a barotropic nonlinear advection process, in which the wave- (synoptic-scale) flow (planetary-scale) interaction plays an very important role. On a favorite planetary-scale flow the certain synoptic-scale disturbance can cause the blocking onset by the interaction of the synoptic-planetary scales. The extended forecasts show that the introduction of the optimal initial vorticity forcing can predict the blocking process up to the 7th or 8th day in this simple model case.

The experimental results in this study show that the 4-dimensional variational approach has a good potential to be applied to study the dynamics of the medium-range weather processes. This simple model case study only is an initial trial. Applying this framework in this study to a complex model will further help understand the mechanism of the atmospheric/oceanic processes and improve their prediction.

# 1 Introduction

Blocking is a persistent anomaly of the large-scale circulation of the atmosphere at middle and high latitudes (Rex 1950; Dole and Gordon 1983). The dynamics of the anomaly circulation have been a hot topic of considerable scientific interest since during blocking the local weather often appears extremes. Many theories exist that try to understand the mechanism of blocking: multiple flow equilibria (Charney and DeVore 1979), instability (Frederiksen 1982), resonance mode (Tung and Lindzen 1979) and low-frequency oscillation (Nakamura and Wallace 1993), etc. It is well known (Berggren et al. 1949; Namias 1964; Standers and Gyakum 1980; Reinhold and Pierrehumbert 1982; Shutts 1983; Tibaldi and Buzzi 1983; Colucci 1985; Colucci and Alberta 1996) that the interaction of synoptic-planetary scales is an important mechanism of the atmospheric blocking.

Efforts (Colucci 1985, 1987; Dole 1989; Tsou and Smith 1990; Lupo and Smith 1993; Colucci and Alberta 1996) have been made to find out the relationship between atmospheric blocking and antecedent, upstream cyclone activities for improving the forecast of blocking events. Colucci and Alberta (1996) from statistics on a great number of cases investigated the preconditioning characteristics of planetary waves. They found that if a lower tropospheric explosive cyclogenesis occurs over a region in which the 50Kpa geostrophic  $u$ ,  $v$  and their anomalies  $u'$  and  $v'$  satisfy that  $v' > 0$ ,  $u' < 0$  and  $v/u > 0.5$  the likelihood of block onset exceeds the climatological expectation within 5 days and  $60^\circ$  degrees of the explosive cyclogenesis. Identifying fast growth modes as the precursor of blocking anomalies is the other aspect of the efforts (Frederiksen 1989; Frederiksen and Bell 1990; Frederiksen 1998).

Since the optimal control theory was introduced into atmospheric numerical analysis (Le Dimet and Talagrand, 1986), the adjoint of a numerical model has been used to calculate the sensitivity of a model aspect. Zou et al. (1993) applied the adjoint sensitivity formalism of Cacuci (1981a,b) into a two-layer isentropic model to examine the sensitivity of blocking index to the initial vorticity sources. This technique was expanded to examine the sensitivity of the efficacy of modal and nonmodal perturbations in causing block onset (Pondeca et al. 1998). Others (Li et al. 1998) used the derived sensitivity information by adjoint equations to approximate the initial vorticity forcing to study block onset.

This study applies a 4-dimensional variational approach to calculate the optimal initial vorticity forcing for block onset and examines the impact of the derived optimal initial vorticity forcing on

blocking simulation and forecast. After a brief description of a global barotropic spectral model and its adjoint in section 2, the relative data and methodology are presented in section 3. The results including the calculated sensitivity distribution using the adjoint equation and the derived optimal initial vorticity forcing by the optimization procedure which combines the nonlinear model, the adjoint and a quasi-Newton minimization algorithm are exhibited in section 4. The section 5 examines the impact of the derived optimal initial vorticity forcing on blocking simulation and forecast. Conclusions and discussions are given in section 6.

## 2 A global barotropic spectral model and its adjoint

### 2.1 A global barotropic spectral (GBS) model

The fundamental of a barotropic model is the barotropic vorticity advection equation. Certain modifications (introduction of the Cressman parameter and the real terrain, for instance) can improve its single level and nondivergency limits. Based on the equation of conservation of potential vorticity (Haltiner and Williams, 1980) with the consideration of terrain effect, a modified barotropic vorticity equation can be written as

$$\frac{\partial}{\partial t}(\nabla^2 - \lambda^2)\psi + J(\psi, \nabla^2\psi) + \beta\frac{\partial\psi}{\partial x} + J(\psi, h') = f_c \quad (1)$$

where  $\psi$  is the geostrophic streamfunction,  $\beta$  is the change rate of the Coriolis parameter with latitudes,  $h' = \frac{f_0}{H_0}h_{terrain}$ , representing the effect of topography and  $f_c$  represents the vorticity forcing. Here  $\lambda^2 = \frac{f^2}{gH_0}$ , is the Cressman parameter,  $f$  the planetary vorticity and  $H_0$  the average atmospheric “equivalent depth.”

When (1) is expanded on a mesh system over the global domain the barotropic model can be written as a matrix form as

$$\frac{\partial\psi}{\partial t} = \mathbf{F}(\psi, \mathbf{f}_c) \quad (2)$$

where  $\mathbf{F}(\psi, \mathbf{f}_c)$  is a matrix notation of reservoir terms in (1). In this study, time integration is only for spectral coefficients in which a rhomboidal 21 truncation is applied for the transformation between spectral coefficients and grid values (for gridpoint model, solving the Helmholtz equation is involved for for each updating time step of the streamfunction  $\psi$ ).  $\mathbf{f}_c$  is the vorticity forcing vector. The Gaussian gridpoints include 54 (latitude)  $\times$  64 (longitude) gridpoints. Like most of numerical models, except that a forward time integration is used for the first time-step (stepsize= 30

minutes), a leap frog time integration scheme is used to forward the model. An Asselin time filter (Asselin 1972) as

$$\psi_t = \frac{1}{2}\epsilon\psi_{t-1} + (1 - \epsilon)\psi_t + \frac{1}{2}\epsilon\psi_{t+1} \quad (3)$$

is applied for damping spurious computational modes.

## 2.2 The TLM and adjoint of the GBS model

For coding the adjoint of the GBS model, first, we differentiate all nonlinear terms in (1) to develop the tangent linear model (TLM). If restricting the control parameters to be initial conditions of the streamfunction and the vorticity forcing, the TLM that governs the evolution of a perturbed state along the trajectory of the basic state can be written as

$$\begin{aligned} \frac{\partial}{\partial t}(\nabla^2 - \lambda^2)\delta\psi + J(\delta\psi, \nabla^2\psi) + J(\psi, \nabla^2\delta\psi) \\ + \beta \frac{\partial\delta\psi}{\partial x} + J(\delta\psi, h') = \delta f_c \end{aligned} \quad (4)$$

or matrix form as

$$\frac{\partial\delta\psi}{\partial t} = \mathbf{F}'_{\psi}(\psi, \mathbf{f}_c)\delta\psi + \mathbf{F}'_{\mathbf{f}_c}(\psi, \mathbf{f}_c)\delta\mathbf{f}_c \quad (5)$$

where a  $\delta(\cdot)$  represents the perturbation and a  $(\cdot)$  represents the basic state.  $\mathbf{F}'_{\psi}(\psi, \mathbf{f}_c)$  and  $\mathbf{F}'_{\mathbf{f}_c}(\psi, \mathbf{f}_c)$  are respectively the first derivatives of  $\mathbf{F}(\psi, \mathbf{f}_c)$  with respect to  $\psi$  and  $\mathbf{f}_c$ . Then we differentiate all nonlinear terms in the GBS model to code the TLM (5). Next, through a “the adjoint of finite difference” approach (Sirkes and Tziperman 1997), we coded adjoints by transposing all DO loops and subroutines in the TLM. If  $L = L_n \cdots L_2 L_1$  represents the propagator of the TLM such as  $\delta\psi_t = L_n \cdots L_2 L_1 \delta\psi_0$ , then a transposed version  $L^* = L_1^* L_2^* \cdots L_n^*$  represents its adjoint. An inner product check such as  $\langle L \delta\psi, L \delta\psi \rangle = \langle \delta\psi, L^* L \delta\psi \rangle$  agreed to 15 decimal digits on 64-bit arithmetic when the model was run at rhomboidal 21 truncation with leap-frog time integration for 120 hours with 30-minute time-step.

## 3 Data and methodology

### 3.1 Two blocking cases

The streamfunctions in this study are derived using the 50kPa  $u$  and  $v$  extracted from ECMWF (European Centre for Medium-Range Weather Forecasts) re-analysis data. Case 1 chosen in this study for block onset is a blocking process occurred during the end of December of 1990 and the

beginning of 1991. Fig. 1 presents the daily evolution of streamfunctions on 50kPa isohypses starting from 00 UTC 28 December 1990. At the end of December of 1990, over the east of the North Pacific maintained a high ridge and over the west of the ridge is a low trough. On 30 December the ridge strengthened and developed to the north. On 31 December an “ $\Omega$ ” pattern blocking was onset over the high-latitude regions in the North Pacific, which centered at the east Siberia and Bering Strait, covered a region south to the Aleutian Islands and north to the Chukchi Sea. This blocking reached its mature phase on 1 January 1991 and the “ $\Omega$ ” pattern had maintained until 3 January. On 4 January the blocking high degraded to a high ridge and gradually weakened further.

Case 2 chosen for this study is a “dipole” pattern blocking process over the east of the North Atlantic and the west coast of the Europe occurred during the early of November 1980. As shown in Fig. 2, at the beginning of November 1980 a high-ridge developed over the west Europe, and over both its downstream and upstream, the central Europe and the central North Atlantic, were two troughs. With the development of these troughs and ridge, a dipole blocking was onset on 5 November 1980 and maintained until 7 November. Afterward the cut-off low and blocking high slightly weakened but maintained 9 November. After 10 November the blocking structure further weakened and degraded to trough and ridge.

### 3.2 The cost function measuring the forecast errors over a local domain

Many investigations have showed that blocking processes have the initial vorticity forcing as pre-conditions (Shutts 1983; Colucci and Alberta 1996; Frederiksen 1998). The real application of these theoretical or empirical postulates is difficult due to the shortage of quantitative accuracy for the location and the amplitude of the vorticity forcing. In order to solve for the precondition of the blocking process, we inversely retrieve the optimal vorticity forcing using a 4-dimensional variational approach. The cost function is defined as a sum of squared forecasting errors of the streamfunctions during the block onset period over a local domain which is occupied by the blocking. Then the cost function can be expressed as

$$J(\mathbf{f}_c) = \frac{1}{2} \sum_{t=t_r}^{t_R} (\boldsymbol{\psi}_{\mathbf{D}}^f - \boldsymbol{\psi}_{\mathbf{D}}^a)^T (\boldsymbol{\psi}_{\mathbf{D}}^f - \boldsymbol{\psi}_{\mathbf{D}}^a) \quad (6)$$

where  $\boldsymbol{\psi}_{\mathbf{D}}^f$ ,  $\boldsymbol{\psi}_{\mathbf{D}}^a$  represent respectively the modeled and analysed streamfunction vectors over the local blocking domain,  $\mathbf{D}$ , as shown by shaded regions in Fig. 3 in which panel *a* represents the case 1 and panel *b* represents the case 2.  $[t_r, t_R]$  is the time window the cost function is defined

on. In this study, the verification time window is set as the last 48 hours of 5-day forecasts. For example, for case 1 and case 2 the cost function represents the sum of squared forecast errors of the streamfunctions from 72-hour to 120-hour starting from 00 UTC 28 December 1990 and 00 UTC 1 November 1980, respectively, over domain  $\mathbf{D}$ . The root mean square (RMS) of the forecast errors of streamfunctions during the 48-hour period is shown in Fig. 3 by thick lines. The time mean of the ECMWF re-analysis streamfunctions from 00 UTC 31 December 1990 to 00 UTC 2 January 1991 (panel *a*), from 00 UTC 4 November 1980 to 00 UTC 6 November 1980 (panel *b*), is also plotted in Fig. 3 by thin lines as the reference.

$\mathbf{f}_c$  in (6) represents a stationary vorticity forcing vector during some initial period (initial 24 hours in this study). Minimizing  $J(\mathbf{f}_c)$  of (6) by adjusting the initial vorticity forcing vector  $\mathbf{f}_c$  is conducting a strong constraint experiment, i.e. under the constraint of the barotropic vorticity advection equation (1), varying the initial vorticity forcing to force the modeled streamfunctions over the local blocking domain close to the re-analysis streamfunctions as much as possible. Through the process we try to understand the importance of the initial vorticity forcing in the formation of blocking processes.

### 3.3 Calculation of the gradient of the cost function

The goal of this study is to find an optimal initial vorticity forcing vector ( $\mathbf{f}_c^{opt}$ ) which minimizes the cost function defined by (6). An adjoint integration backward in time evaluates the gradient of the cost function with respect to the initial vorticity forcing ( $\nabla_{\mathbf{f}_c} J$ ). This process can be symbolically written as

$$-\frac{\partial \hat{\mathbf{f}}_c}{\partial t} - \left( \frac{\partial \mathbf{F}(\psi, \mathbf{f}_c)}{\partial \mathbf{f}_c} \right)^T \hat{\mathbf{f}}_c = \psi_{\mathbf{D}}^f - \psi_{\mathbf{D}}^a$$

$$\nabla_{\mathbf{f}_c} J = \int_{t_R}^{t_0} \hat{\mathbf{f}}_c dt \quad (7)$$

where  $\hat{\mathbf{f}}_c$  is the adjoint variable related to the initial vorticity forcing vector  $\mathbf{f}_c$ . As an application of the chain rule the adjoint integration efficiently evaluates the gradient of the cost function with respect to control variables although the tangent linear approximation may not validly describe the evolution of a small perturbation (Zhang et al. 2000) for a long forecast leading time. Therefore, we can use the adjoint model to evaluate the gradient of  $J$  in (6) defined by forecasts out of 5 days with respect to the initial vorticity forcing ( $\mathbf{f}_c$ ).

A gradient test is necessary in order to guarantee the gradient calculated from the adjoint

integration is correct. From the first order approximation of the Taylor expansion of the cost function, one defines a ratio to measure the consistency between the linear increment along the gradient direction of  $J$  and a perturbed  $J$  (Navon et al. 1992) as

$$\Phi(\alpha) = \frac{J(\mathbf{f}_c + \alpha \mathbf{e}) - J(\mathbf{f}_c)}{\alpha \mathbf{e}^T \nabla_{\mathbf{f}_c} J} = 1 + O(\alpha) \quad (8)$$

where  $\alpha$  is a small scalar governing the magnitude of perturbations and  $\mathbf{e}$  is a unit vector such as  $\mathbf{e} = -\nabla_{\mathbf{f}_c} J / \|\nabla_{\mathbf{f}_c} J\|^{-1} \times 10^{-9}$ . (8) shows that when  $\alpha$  is small, for a correct gradient  $\nabla_{\mathbf{f}_c} J$ ,  $\Phi(\alpha)$  goes to 1 as  $\alpha$  is small but not a machine zero. We choose the period from 00 UTC 31 December 1990 to 00 UTC 2 January 1991 as the blocking onset phase and use 00 UTC 28 December 1990 as the initial condition to carry out the gradient test as (8) to form Fig. 4 which presents the curve of the logarithm of  $\Phi(\alpha) - 1$  with respect to  $\log_{10}\alpha$ . Figure 4 shows that the adjoint integration correctly calculates the gradient of  $J(\mathbf{f}_c)$  with respect to the initial vorticity forcing vector  $\mathbf{f}_c$  since a linear increment of  $J$  along the derived gradient direction always sufficiently represents the perturbed cost function by  $\alpha \mathbf{e}$  as  $\alpha = 10^{-14} - 10^{-1}$ .

Once the gradient of  $J(\mathbf{f}_c)$  is available, we will employ a limited memory quasi-Newton algorithm (Liu and Nocedal 1989) to minimize  $J(\mathbf{f}_c)$  with respect  $\mathbf{f}_c$  so as to solve for the optimal initial vorticity forcing, in section 4.2.

## 4 Numerical results

### 4.1 The sensitivity distribution of blocking with respect to the initial vorticity forcing

Using the analysis streamfunctions at 00 UTC 28 December 1990 (case 1) and 00 UTC 1 November 1980 (case 2) from the ECMWF re-analysis data as initial conditions, the nonlinear GBS model is first integrated up to 5 days without the vorticity forcing to calculate the  $J$  by (6) using the last 48-hour (from 72-hour to 120-hour) forecasted streamfunctions. Then the adjoint model is integrated backward in time by collecting the first derivatives of  $J$  with respect to the modeled streamfunction in this 48-hour time window as input. While the time of the integration goes back to the initial time the adjoint variable  $\delta \hat{\mathbf{f}}_c$  represents the gradient of  $J$  with respect to the initial vorticity forcing,  $\mathbf{f}_c$ , by (7). If the adjoint variable of  $\delta \hat{\mathbf{f}}_c$  is accumulated over the initial 24 hours, distributions of the calculated gradient tell us where and how much is sensitive to the blocking onset if a stationary vorticity forcing is put in during the initial 24 hours.

Figure 5 displays the sensitivity distributions of the blocking onset in two cases (panel *a* for case 1 and panel *b* for case 2) with respect to the initial 24-hour vorticity forcing. The time mean of the analysis streamfunctions over the 48 hours is plotted as the reference for both cases. Both panels show that the negative sensitivity is located over the south and the west of the blocking while over the blocking region and the east of blocking region is always the positive sensitivity. Since these sensitivity distributions are derived as the initial vorticity forcing is zero, the positive/negative sensitivity always means a negative/positive vorticity forcing is needed over the corresponding regions. Therefore, these negative/positive sensitivity distributions reflect the positive/negative vorticity demand for the blocking onset. This kind of initial vorticity forcing representing a synoptic scale disturbance can generate and transport the positive/negative vorticity to trigger and maintain the block. From Fig. 5, it is observed that for the “ $\Omega$ ” pattern blocking case (panel *a*) the strength of positive/negative sensitivity is almost even while for the “dipole” pattern blocking case (panel *b*) the strength of positive sensitivity is much less than that of negative sensitivity. This means that to form the “dipole” blocking the developing of trough at the southwest of the blocking is much more important than the strengthening of the ridge itself.

## 4.2 Minimization of the cost function

The sensitivity distributions shown in section 4.1 provide the possible locations of the initial vorticity forcing to form blocking. However due to the constraint of the barotropic vorticity advection over the global domain, only using the sensitivity distribution at  $\mathbf{f}_c = 0$  is not sufficient to derive the distribution of the initial vorticity forcing. In this section, an iterative optimization procedure using the limited memory quasi-Newton method (Liu and Nocedal 1989) is employed to solve for the optimal initial vorticity forcing for each case.

In the minimization procedure, each iteration includes a nonlinear GBS model run (evaluate  $J$ ), an adjoint model run (evaluating  $\nabla_{\mathbf{f}_c} J$ ) and an optimization search process. Starting from  $\mathbf{f}_c = 0$  (iteration 0), the decreases of the cost function ( $J$ , thick-solid line) and the norm of the gradient ( $\|\nabla_{\mathbf{f}_c} J\|$ , solid line) and RMSE (dashed line) over the 48-hour time window with the iteration number are displayed in Fig. 6 for case 1 (panel *a*) and case 2 (panel *b*). About through 10–12 iterations, for both cases the cost functions decrease by 95%, and the norm of the gradient reduces by two order and RMSE reduces by one order. Then due to the constraint of the global vorticity advection the norm of the gradient and RMSE stay at the same order level (decrease very little as

the iteration proceeds).

### 4.3 Optimal initial vorticity forcings

The optimal initial vorticity forcing solved from the optimization iterative procedure described in section 4.2 is showed in Fig. 7. Panel *a* and panel *b* respectively display the distributions of the optimal initial vorticity forcing  $\mathbf{f}_c^{opt}$  for case 1 and case 2. The initial streamfunctions (00 UTC 28 December 1990 for case 1 and 00 UTC 1 November 1980 for case 2) are plotted as a background in both panels. Comparing Fig. 7 with Fig. 5, we found that the distributions of the positive/negative  $\mathbf{f}_c^{opt}$  (Fig. 7) are overall similar to the sensitivity distributions (Fig. 5) with opposite phases. This is consistent with analyses in section 4.1, i.e., again the gradient (sensitivity)  $\|\nabla_{\mathbf{f}_c} J\|$  shown in Fig. 5 is evaluated as  $\mathbf{f}_c = 0$ . This phenomenon suggests if an appropriate scalar is chosen, to some accuracy, the opposite phase of the gradient may be served as an approximation of the vorticity forcing.

In the dynamics of barotropic vorticity advection, the derived initial vorticity forcing serves as a synoptic-scale disturbance on the planetary trough/ridge motions. Fig. 7 indicates that for both cases the negative (anticyclonic vortex) initial vorticity forcing distributes over the blocking high region and the positive (cyclonic vortex) initial vorticity forcing distributes along the upstream low troughs. Over the downstream low troughs in both cases the central regions are the positive (cyclonic vortex) initial vorticity forcing. Those cyclonic/anticyclonic vorticity sources favor the development of the anticyclonic vortex over the blocking high and the cyclonic vortex at its upstream/downstream. However, for the dipole pattern blocking (case 2), a big cyclonic vorticity forcing center distributes over the cut-off low center and its southeast region (the trough bottom) while for the  $\Omega$  block pattern (case 1) at the trough bottom is weak anticyclonic vorticity forcing. This is consistent with the requirement of a stronger cyclonic vorticity advection to form a cut-off low center over the south of the blocking high for this blocking pattern.

In addition, it seems that the location of the greatest positive vorticity forcing center for case 1 falls in the region described by Colucci and Alberta (1996) (panel *a* in Fig. 7), i.e.  $v' > 0$ ,  $u' < 0$  and  $v/u > 0.5$ . For both cases, a few large vorticity forcing centers are located over tropics/subtropics. Since the derived vorticity forcing includes all factors that the dynamics of the barotropic vorticity advection fails to describe such as baroclinic disturbance, vertical advection, etc. physically interpreting the derived vorticity forcing centers requires further study, including

use of more complex models.

In next section, we will show that using these derived vorticity forcings as the initial 24-hour synoptic-scale perturbations on the initial streamfunction fields (00 UTC 28 December 1990 for case 1 and 00 UTC 1 November 1980 for case 2), the barotropic nonlinear advection process can reconstructs the onset of these blocking processes.

## 5 Impact of the optimal initial vorticity forcing on blocking simulation and forecasts

### 5.1 Reconstruction of the blocking onset processes

Using the derived optimal initial vorticity forcing (thick lines) shown in Fig. 7, we run the barotropic model again (the initial conditions are same as before) and make 10-day forecasts for both cases (the forecasts with/without the optimal initial vorticity forcing are called the optimal/control forecasts, hereafter). The first 5-day control (left column) and optimal (right column) forecasts for case 1 and case 2 are exhibited in Fig. 8 and Fig. 9, respectively. Comparing these forecasts with the corresponding analyses in Fig. 1 (case 1) and Fig. 2 (case 2), it is observed that for both cases the introduction of the optimal initial vorticity forcing mostly reconstructs the process of the block onset while the control forecasts entirely lose the capability to describe the strengthening ridge which develops into a blocking high (for both cases), and/or a deepening trough which develops into a cut-off low center at the right phase(for case 2).

The reconstruction of the block onset above using the derived initial vorticity forcing tells us that the formation of blocking can be mostly described by a barotropic nonlinear advection process. In the process, the wave- (synoptic-scale) flow (planetary-scale) interaction plays an very important role. On a favorite planetary-scale flow the certain synoptic-scale disturbance can cause the block onset by the interaction of the synoptic-planetary scales.

### 5.2 Improvement of blocking forecasts

In order to examine the impact of the optimal initial vorticity forcing on the forecast of the blocking events by the barotropic model, both control and optimal forecasts are extended up to 10 days. Figure 10 presents the daily evolution of case 1 (left panels) and case 2 (right panels) forecasts from day 6 to day 10. From Fig. 10, it is observed that for case 1 with the optimal initial vorticity

forcing the phase of the forecasted blocking high (high ridge) over Bering Sea is traceable until 10 days although the phase is lagged to the analysis from day 6 on, and the trough over the west of America continent is greatly exaggerated. For case 2, although the trough of optimal forecasts over the northern Atlantic is exaggerated, the blocking high over the west of the North Atlantic is traceable up to 8 days. Of course, the control forecasts do not have any traceable ridge or trough during the whole period. These results show that although the barotropic vorticity advection dynamics is only an approximate description (probably leading order), rather than a complete picture of the complex blocking mechanism (baroclinic processes, for instance), the optimal vorticity forcings derived from a 4-dimensional variational approach have certain capability to improve forecasts. The optimization process in the 4-dimensional variational approach accounts all unresolved processes by the simplified dynamics as the vorticity forcing term, so as to simplify the complexity, to some degree. Once the optimal vorticity forcings in terms of favorites to blocking onset or development are derived, the forced barotropic vorticity model is able to extend the valid forecasts.

## 6 Summary and discussions

With the aid of a global barotropic model, the role of the interaction of the synoptic-scale disturbance and the planetary flow in block onset is examined by a 4-dimensional variational approach in this study. A cost function is defined to measure the squared errors of the forecasted streamfunctions during block onset period, over a selected blocking domain. The sensitivity of the block onset with respect to the initial synoptic-scale disturbance is studied by examining the gradient of the defined cost function with respect to the initial (the first 24 hours, in this study) vorticity forcing, which is evaluated by the adjoint integration. The distribution of the sensitivity superposed on the initial streamfunction tells us the possible need of the synoptic disturbance over a favorite planetary flow for the block onset. Furthermore, connecting the evaluation of the defined cost function and the gradients with the limited memory quasi-Newton optimization algorithm (Liu and Nocedal 1989) the optimal initial vorticity forcing for the block onset is solved by the iterative minimization procedure.

For two studied cases the introduction of the optimal initial vorticity forcing into the nonlinear barotropic vorticity advection process mostly reconstructs the process of the block onset. This phenomenon tells us that although the onset and development of blocks is a rather complex process with many factors involved, the nonlinear barotropic vorticity advection process can be treated as

the leading order approximation. In the process, the wave- (synoptic-scale) flow (planetary-scale) interaction plays an very important role. On a favorite planetary-scale flow the certain synoptic-scale disturbance can cause the block onset by the interaction of the synoptic-planetary scales. The extended forecasts up to 10 days show that the introduction of the optimal initial vorticity forcings derived from the 4-dimensional variational approach can extend the valid forecasts 2 to 3 days in this simple model study case.

The experimental results in this study show that the 4-dimensional variational approach has a good potential to be applied to study the dynamics of the medium-range weather processes. However under the framework of the barotropic vorticity advection, the derived vorticity forcing blends all factors that the dynamics of the barotropic vorticity advection unresolves. It's very difficult to connect the dervied forcing distribution with the real atmospheric forcing distribution due to the model bias. This simple model case only is an initial trial. Applying the framework in this study to a complex model will further help understand the mechanism of the atmospheric/oceanic processes and improve their forecasting.

In addition, it's worth to mention that the derived results through this 4-dimentional variational approach may have some dependency on the definition of the cost function (Frederiksen 2000). This study only use a sum of squared forecasting errors of the streamfunctions as a distance measurement of the model simulation and "observations." In the future, a throughout examination of the dependency of the derived optimal vorticity forcing on the definition of the cost function needs to be done for further application of this approach.

#### *Acknowledgements*

Except that the initial codes of the forward barotropic model was provided by Dr. JonE Ahlquist, authors would thank Dr. JonE Ahlquist for his generous discussions and suggestions during this study. Authors thank Dr. H. Wang for her comments on earlier versions of this manuscript. Thanks go to two anonymous reviewers for thorough and helpful comments and suggestions.

## REFERENCES

- Berggren, R., B. Bolin, and C. G. Rossby, 1949: An aerological study of zonal motion, its perturbation and breakdown. *Tellus*, **1**, 14–37.
- Cacuci, D. G., 1981a: Sensitivity theory for nonlinear systems. I: Nonlinear functional analysis approach. *J. Math. Phys.*, **22**, 2794–2802.
- , 1981b: Sensitivity theory for nonlinear systems. II: Extensions to additional classes of responses. *J. Math. Phys.*, **22**, 2803–2812.
- , 1988: The forward and adjoint methods of sensitivity analysis. *Uncertainty Analysis*, Yigal Ronen, Ed., CRC Press, Inc., 71–144.
- Charney, J. G., and J. G. DeVore, 1979: Multiple flow equilibria in the atmosphere and blocking. *J. Atmos. Sci.*, **36**, 1205–1216.
- Colucci, S. J., 1985: Explosive cyclogenesis and large-scale circulation changes: Implications for atmospheric blocking. *J. Atmos. Sci.*, **42**, 2701–2717.
- , 1987: Comparative diagnosis of blocking versus nonblocking planetary-scale circulation changes during synoptic-scale cyclogenesis. *J. Atmos. Sci.*, **44**, 124–139.
- Colucci, S. J. and T. L. Alberta, 1996: Planetary-scale climatology of explosive cyclogenesis and blocking. *Mon. Wea. Rev.*, **124**, 2509–2520.
- Dole, R. M., 1989: Life cycles of persistent anomalies. Part I: Evolution of 500 mb height fields. *Mon. Wea. Rev.*, **117**, 177–211.
- Dole, R. M., and N. D. Gordon, 1983: Persistent anomalies of the extra-tropical northern hemisphere wintertime circulation: Geographical distribution and regional persistence characteristics. *Mon. Wea. Rev.*, **111**, 1567–1586.
- Frederiksen J. S., 1982: A unified three-dimensional instability theory of the onset of blocking and cyclogenesis. *J. Atmos. Sci.*, **39**, 969–982.
- Frederiksen J. S., 1989: The role of instability during the onset of blocking and cyclogenesis in Northern Hemisphere synoptic flows. *J. Atmos. Sci.*, **46**, 1076–1092.
- Frederiksen J. S., 1998: Precursors to blocking anomalies: The tangent linear and inverse problem. *J. Atmos. Sci.*, **55**, 2419–2436.

- Frederiksen J. S., 2000: Singular vectors, finite-time normal modes, and error growth during blocking. *J. Atmos. Sci.*, **57**, 312–333.
- Frederiksen J. S., and R. C. Bell, 1990: North Atlantic blocking during January 1979: Linear theory. *Quart. J. Roy. Meteor. Soc.*, **116**, 1289–1313.
- Haltiner, G. J. and R. T. Williams, 1980: Numerical prediction and dynamic meteorology, 2nd ed., Wiley and Sons, 477 pp.
- LeDimet, F. X. and O. Talagrand, 1986: Variational algorithms for analysis and assimilation of Meteorological observations: Theoretical aspects. *Tellus*, **38A**, 97–110.
- Li Z., A. Barcilon, I. M. Navon, 1999: Study of block onset using sensitivity perturbation in climatological flows. *Mon. Wea. Rev.*, **127**, 879–900.
- Liu, D. C., and J. Nocedal, 1989: On the limited memory BFGS method for large scale optimization. *Mathematical Programming* , **45**, 503–528.
- Lupo, A. R., and P. J. Smith, 1995: Climatological features of blocking anticyclones and precursor extratropical cyclones. *Tellus*, **47**, 439–456.
- Nakamura, H., and J. M. Wallace, 1990: Observed changes in baroclinic wave activity during the life cycles of low-frequency circulation anomalies. *J. Atmos. Sci.*, **47**, 1100–1116.
- Namias, J., 1964: Seasonal persistence and the recurrence of European blocking during 1958–60. *Tellus*, **16**, 394–407
- Navon, I. M., X. Zou, J. Derber, and J. Sela, 1992: Variational data assimilation with an adiabatic version of the NMC spectral model. *Mon. Wea. Rev.*, **120**, 1433–1446.
- Pondeca, M.S. F., A. Barcilon and X. Zou, 1998: An adjoint sensitivity study of the efficacy of modal and nonmodal perturbations in causing model block onset. *J. Atmos. Sci.*, **55**, 2095–2118.
- Reinhold, B. P., and R. J. Pierrehumbert, 1982: Dynamics of weather regimes: Quasi-stationary waves and blocking. *Mon. Wea. Rev.*, **110**, 1105–1145
- Rex, D. F., 1950: Blocking action in the middle troposphere and its effect upon regional climate. II: The climatology of blocking action. *Tellus*, **2**, 275–301.
- Sanders, F., and J. Gyakum, 1980: The synoptic-dynamic climatology of the bomb. *Mon. Wea. Rev.*, **108**, 1589–1606.

- Shutts, G. J., 1983: The propagation of eddies in diffluent jet streams: Eddy forcing of “blocking” flows fields. *Quart. J. Roy. Meteor. Soc.*, **109**, 737–762.
- Sirkes, Z. and E. Tziperman, 1997: Finite difference of adjoint or adjoint of finite difference. *Mon. Wea. Rev.*, **125**, 3373–3378.
- Tibaldi, S., and A. Buzzi, 1983: Effects of orography on Mediterranean lee cyclogenesis and its relationship to European blocking. *Tellus*, **35A**, 269–286.
- Tsou, C. H., and P. J. Smith, 1990: The role of synoptic/planetary-scale interactions during the development of a blocking anticyclone. *Tellus*, **42A**, 174–193.
- Tung, K. K. and R. S. Lindzen, 1979: A theory of stationary long waves. Part I: A simple theory of blocking. *Mon. Wea. Rev.*, **107**, 714–734.
- Zhang, S. and X. Zou, 1999: Further discussions on the use of adjoint of discontinuous model physics in 4D-Var. *Submitted to Tellus*.
- Zou, X., A. Barcilon, I. M. Navon, J. Whitaker and D. G. Cacuci, 1993: An adjoint sensitivity study of blocking in a two-layer isentropic model. *Mon. Wea. Rev.*, **121**, 2833–2857.

## FIGURE CAPTIONS

**Fig. 1** Daily evolution of the streamfunction from 00 UTC 28 December 1990 to 00 UTC 6 January 1991 over the domain of  $0\text{--}90^\circ\text{N}$ ,  $120^\circ\text{E}\text{--}270^\circ\text{E}$ . The contours are in  $10^7 m^2 s^{-1}$ .

**Fig. 2** Same as Fig. 1, except from 00 UTC 1 November 1980 to 00 UTC 10 November 1980 and the domain of  $0\text{--}90^\circ\text{N}$ ,  $60^\circ\text{W}\text{--}60^\circ\text{E}$ .

**Fig. 3** Distributions of the time mean of forecast errors (thick) from 72-hour to 120-hour with the initial conditions at a) 00 UTC 28 December 1990 and b) 00 UTC 1 November 1980 over the North hemisphere. Distributions of the time mean of analysis streamfunctions (thin) a) from 00 UTC 31 December 1990 to 00 UTC 2 January 1991 and b) from 00 UTC 4 to 00 UTC 6 November 1980 plotted as the background. The contours are in  $10^6 m^2 s^{-1}$  (solid) and  $10^7 m^2 s^{-1}$  (thin). The shaded region marked by the symbol “D” is the selected domain on which the cost function is defined for block onset.

**Fig. 4** Change of  $\log_{10}[\Phi(\alpha) - 1]$  with  $\log_{10}\alpha$  for the gradient test.

**Fig. 5** Same as Fig. 3, except for the gradient (thick) of the cost function with respect to the initial vorticity forcing. The contours are in  $10^{22} m^4$ . The time mean analysis streamfunctions (thin) in the corresponding time window are plotted as background by contours in  $10^7 m^2 s^{-1}$ , for each case.

**Fig. 6** Changes of the cost function (thick-solid), the norm of the gradient of the cost function with respect to the initial vorticity forcing (thin-solid) and the root mean square of errors (RMSE) (dotted) with the iteration number in minimization using the streamfunctions at a) 00 UTC 28 December 1990 and b) 00 UTC 1 November 1980 as initial conditions.

**Fig. 7** Same as Fig. 3, except for the optimal initial vorticity forcing (thick-solid). The contours are in  $10^{-5} s^{-2}$  and the shaded represents the areas greater than  $2 \times 10^{-5} s^{-2}$ . The initial streamfunctions at a) 00 UTC 28 December 1990 and b) 00 UTC 1 November 1980 are plotted by contours in  $10^7 m^2 s^{-1}$  as background.

**Fig. 8** Daily sequences of the streamfunctions of control forecasts (without the initial vorticity forcing) (left) and optimal forecasts (with the optimal initial vorticity forcing) (right) using the analysis streamfunction at 00 UTC 28 December 1990 as initial conditions, from day 1 to

day 5, over the domain of  $0\text{--}90^\circ\text{N}$ ,  $120^\circ\text{E}\text{--}270^\circ\text{E}$ . The contours are in  $10^7 m^2 s^{-1}$ . The shaded represents the areas greater than  $-4 \times 10^7 m^2 s^{-1}$ .

**Fig. 9** Same as Fig. 8, except for using the analysis at 00 UTC 1 November 1980 as initial conditions, over the domain of  $0\text{--}90^\circ\text{N}$ ,  $60^\circ\text{W}\text{--}60^\circ\text{E}$  and that the shaded represents the areas greater than  $-2 \times 10^7 m^2 s^{-1}$ .

**Fig. 10** Same as Fig. 8, except for the optimal forecasts from day 6 to day 10 using the analysis streamfunctions at 00 UTC 28 December 1990 over the domain of  $0\text{--}90^\circ\text{N}$ ,  $120^\circ\text{E}\text{--}270^\circ\text{E}$  (left) and 00 UTC 1 November 1980 over the domain of  $0\text{--}90^\circ\text{N}$ ,  $60^\circ\text{W}\text{--}60^\circ\text{E}$  (right) as initial conditions, and that the shaded represents areas greater than  $-4 \times 10^7 m^2 s^{-1}$  (left) and  $-2 \times 10^7 m^2 s^{-1}$  (right).

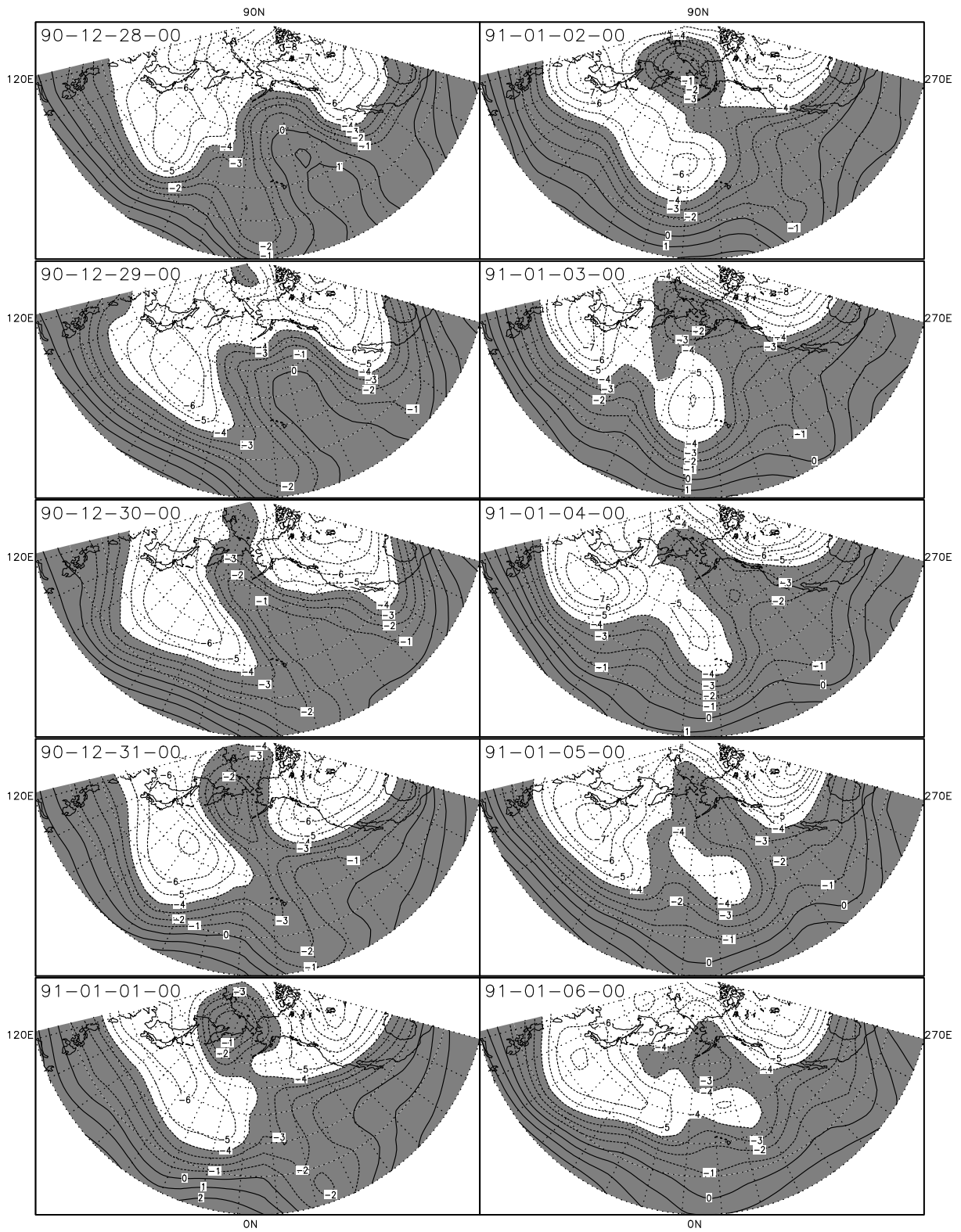


Figure 1: Daily evolution of the streamfunction from 00 UTC 28 December 1990 to 00 UTC 6 January 1991 over the domain of 0–90°N, 120°E–270°E. The contours are in  $10^7 m^2 s^{-1}$ .

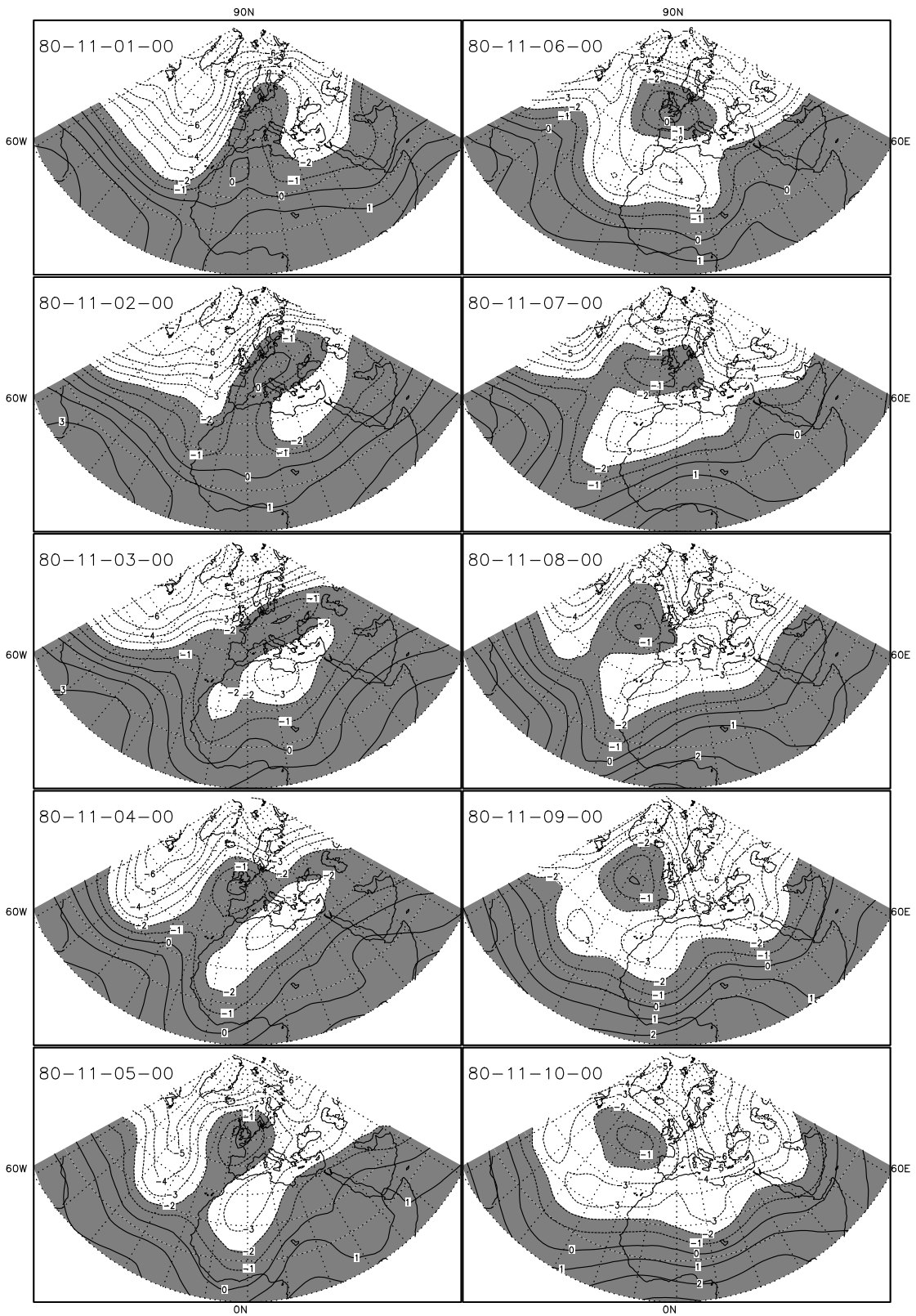


Figure 2: Same as Fig. 1, except from 00 UTC 1 November 1980 to 00 UTC 10 November 1980 and the domain of 0–90°N, 60°W–60°E.

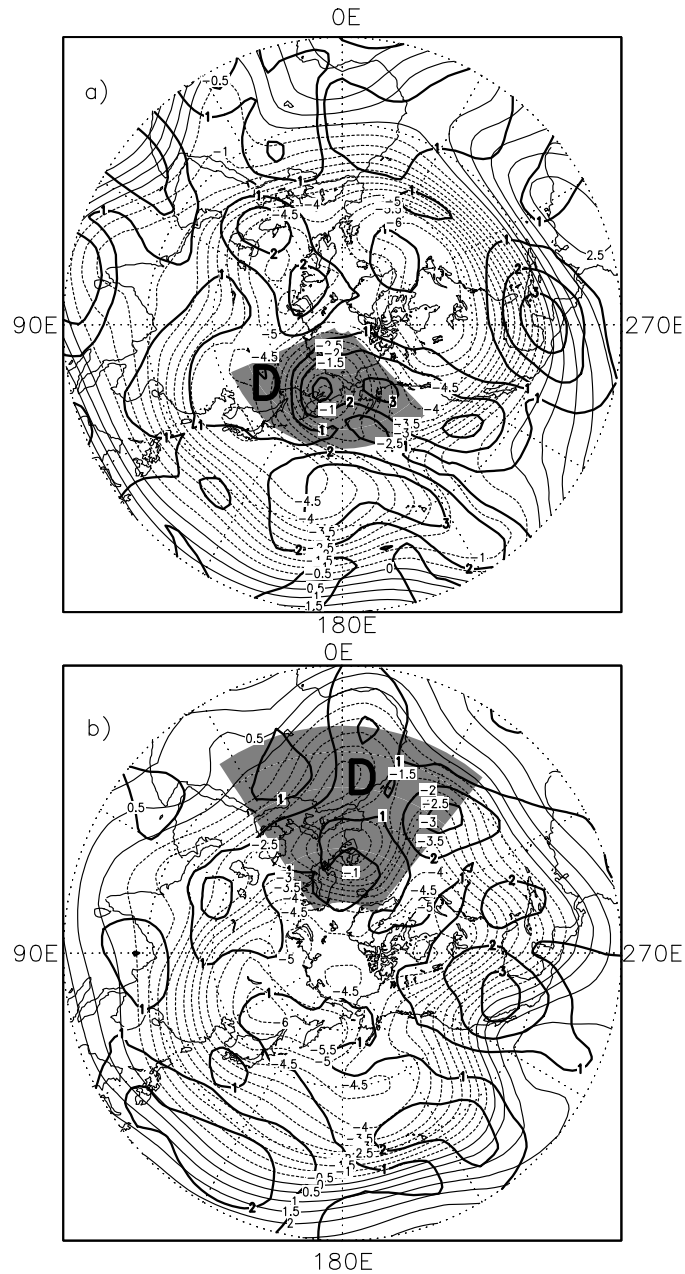


Figure 3: ]Distributions of the time mean of forecast errors (thick) from 72-hour to 120-hour with the initial conditions at a) 00 UTC 28 December 1990 and b) 00 UTC 1 November 1980 over the North hemisphere. Distributions of the time mean of analysis streamfunctions (thin) a) from 00 UTC 31 December 1990 to 00 UTC 2 January 1991 and b) from 00 UTC 4 to 00 UTC 6 November 1980 plotted as the background. The contours are in  $10^6 m^2 s^{-1}$  (solid) and  $10^7 m^2 s^{-1}$  (thin). The shaded region marked by the symbol “D” is the selected domain on which the cost function is defined for block onset.

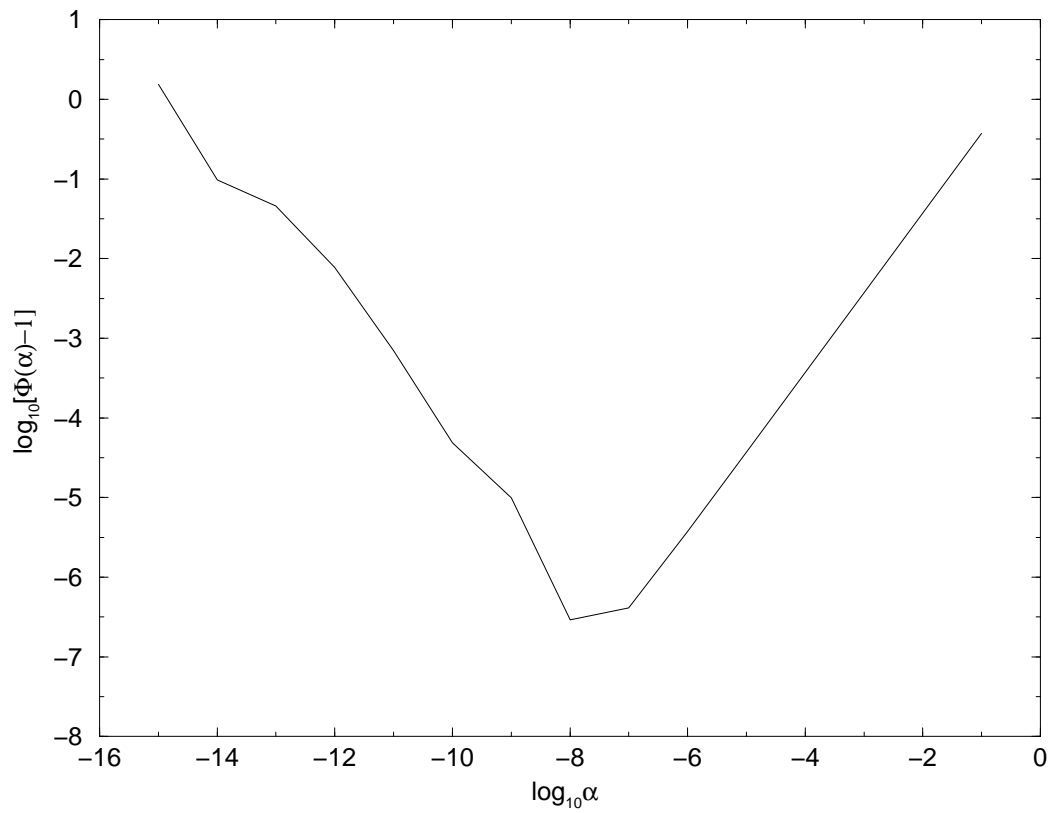


Figure 4: Change of  $\log_{10}[\Phi(\alpha) - 1]$  with  $\log_{10}\alpha$  for the gradient test.

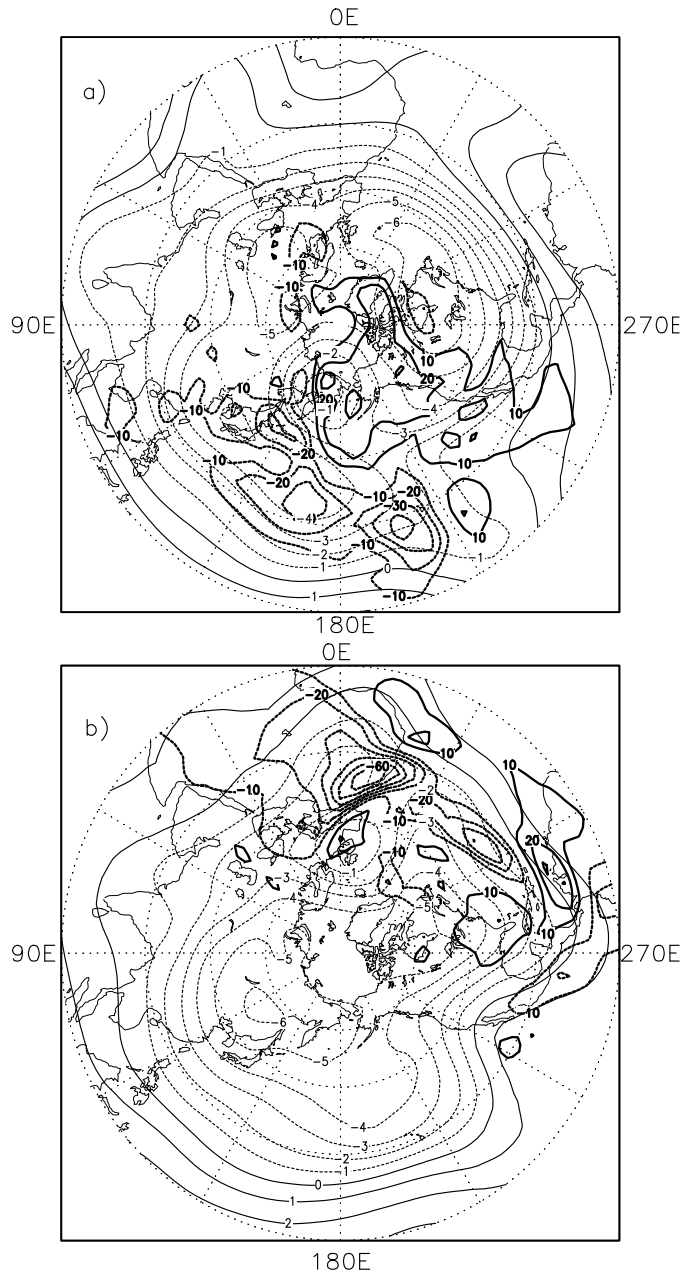


Figure 5: Same as Fig. 3, except for the gradient (thick) of the cost function with respect to the initial vorticity forcing. The contours are in  $10^{22}m^4$ . The time mean analysis streamfunctions (thin) in the corresponding time window are plotted as background by contours in  $10^7m^2s^{-1}$ , for each case.

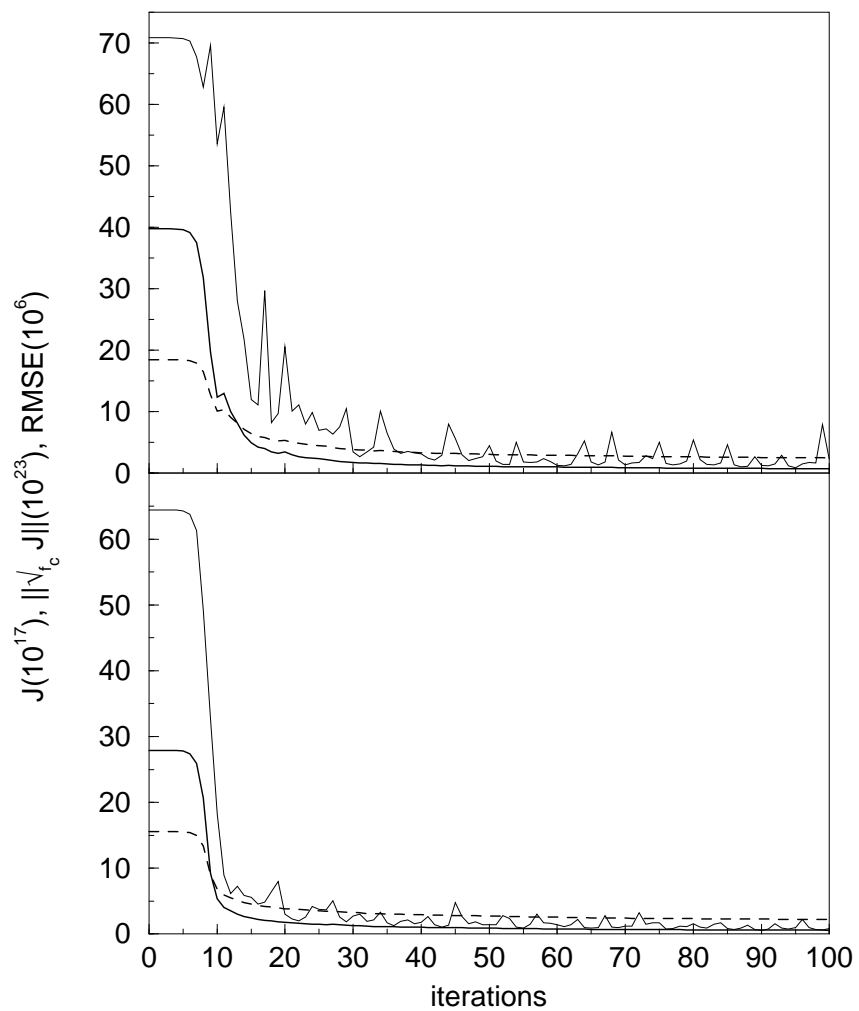


Figure 6: Changes of the cost function (thick-solid), the norm of the gradient of the cost function with respect to the initial vorticity forcing (thin-solid) and the root mean square of errors (RMSE) (dotted) with the iteration number in minimization using the streamfunctions at a) 00 UTC 28 December 1990 and b) 00 UTC 1 November 1980 as initial conditions.

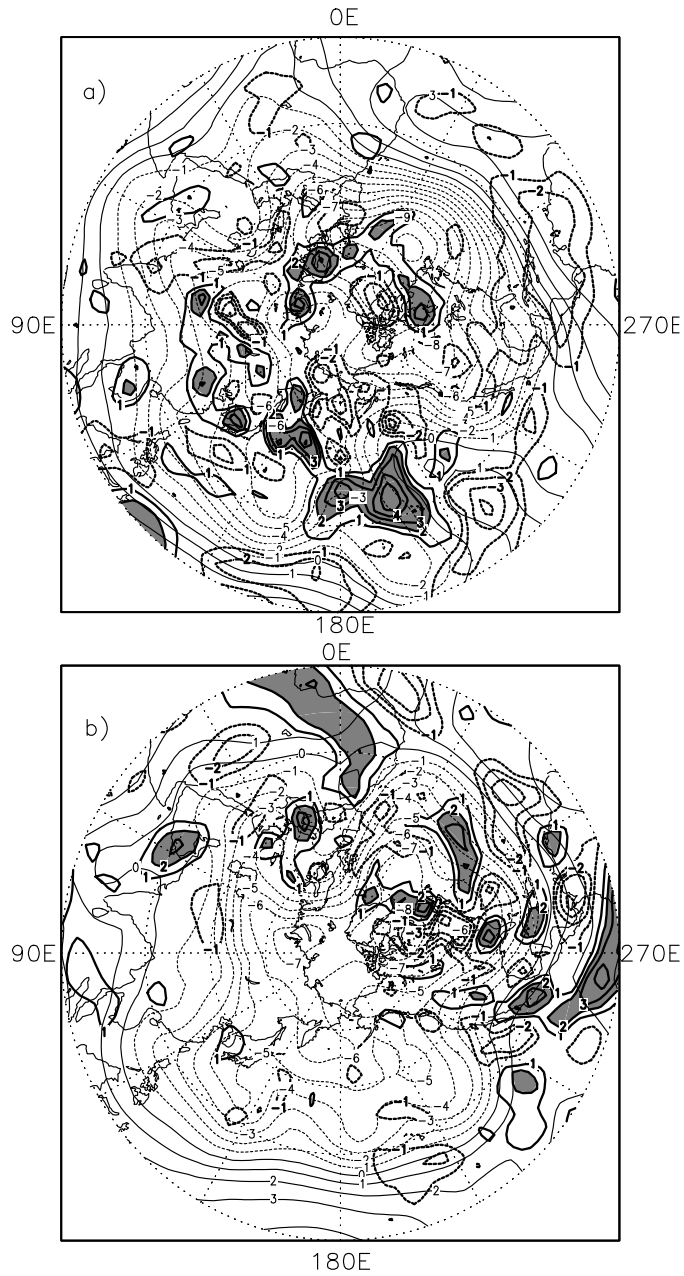


Figure 7: Same as Fig. 3, except for the optimal initial vorticity forcing (thick-solid). The contours are in  $10^{-5} s^{-2}$  and the shaded represents the areas greater than  $2 \times 10^{-5} s^{-2}$ . The initial stream-functions at a) 00 UTC 28 December 1990 and b) 00 UTC 1 November 1980 are plotted by contours in  $10^7 m^2 s^{-1}$  as background.

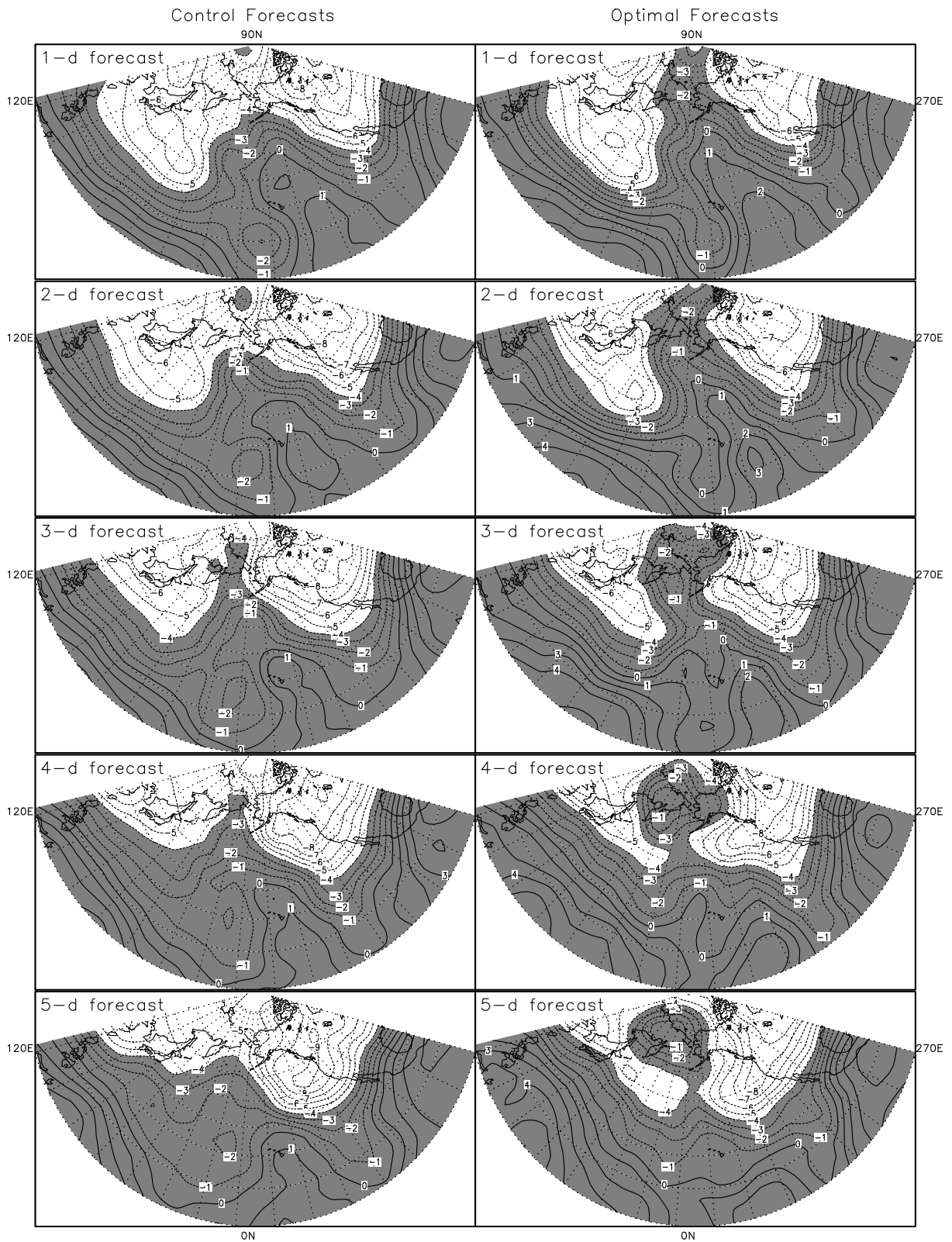


Figure 8: Daily sequences of the streamfunctions of control forecasts (without the initial vorticity forcing) (left) and optimal forecasts (with the optimal initial vorticity forcing) (right) using the analysis streamfunction at 00 UTC 28 December 1990 as initial conditions, from day 1 to day 5, over the domain of  $0-90^{\circ}\text{N}$ ,  $120^{\circ}\text{E}-270^{\circ}\text{E}$ . The contours are in  $10^7 m^2 s^{-1}$ . The shaded represents the areas greater than  $-4 \times 10^7 m^2 s^{-1}$ .

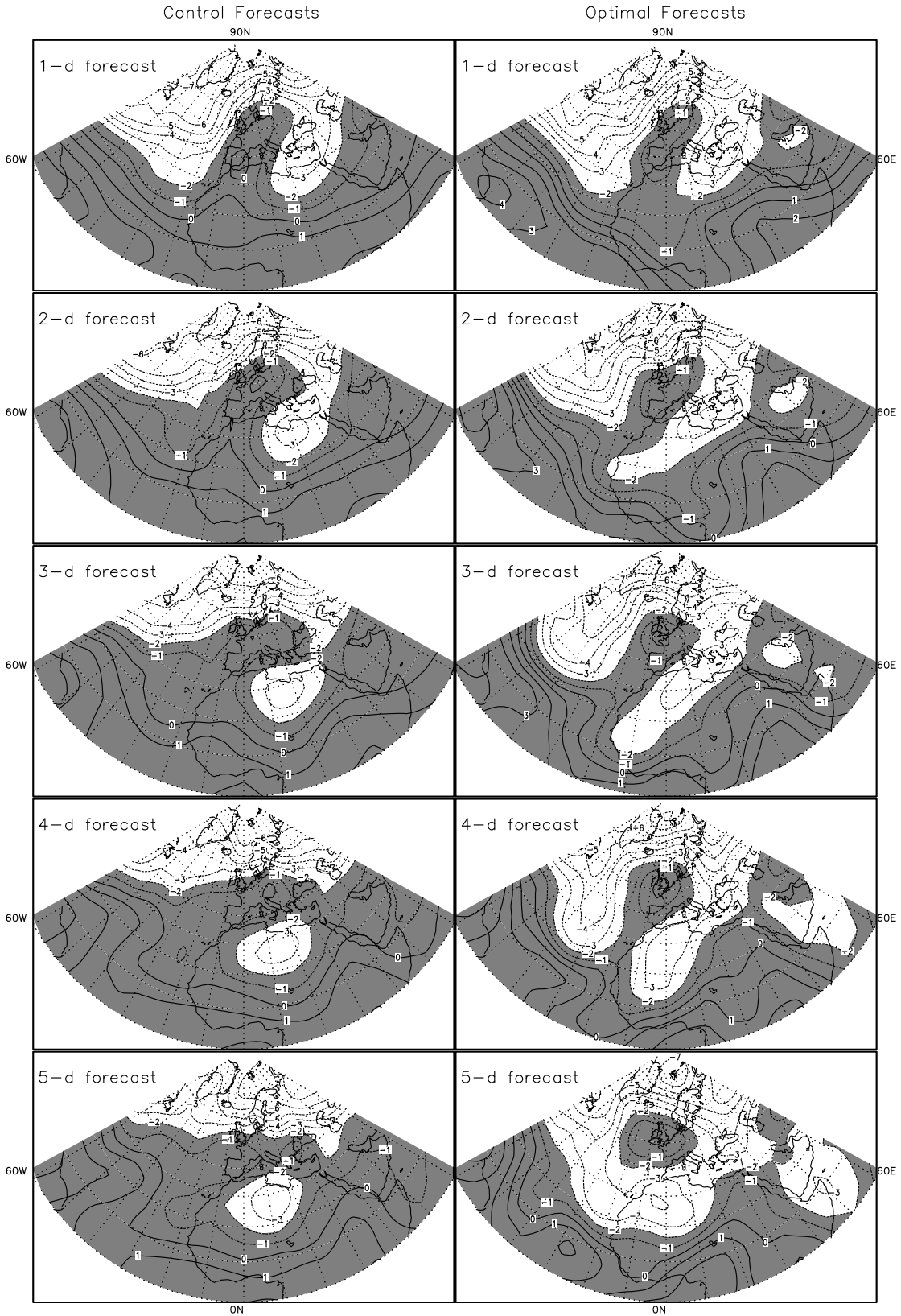


Figure 9: Same as Fig. 8, except for using the analysis at 00 UTC 1 November 1980 as initial conditions, over the domain of 0–90°N, 60°W–60°E and that the shaded represents the areas greater than  $-2 \times 10^7 m^2 s^{-1}$ .

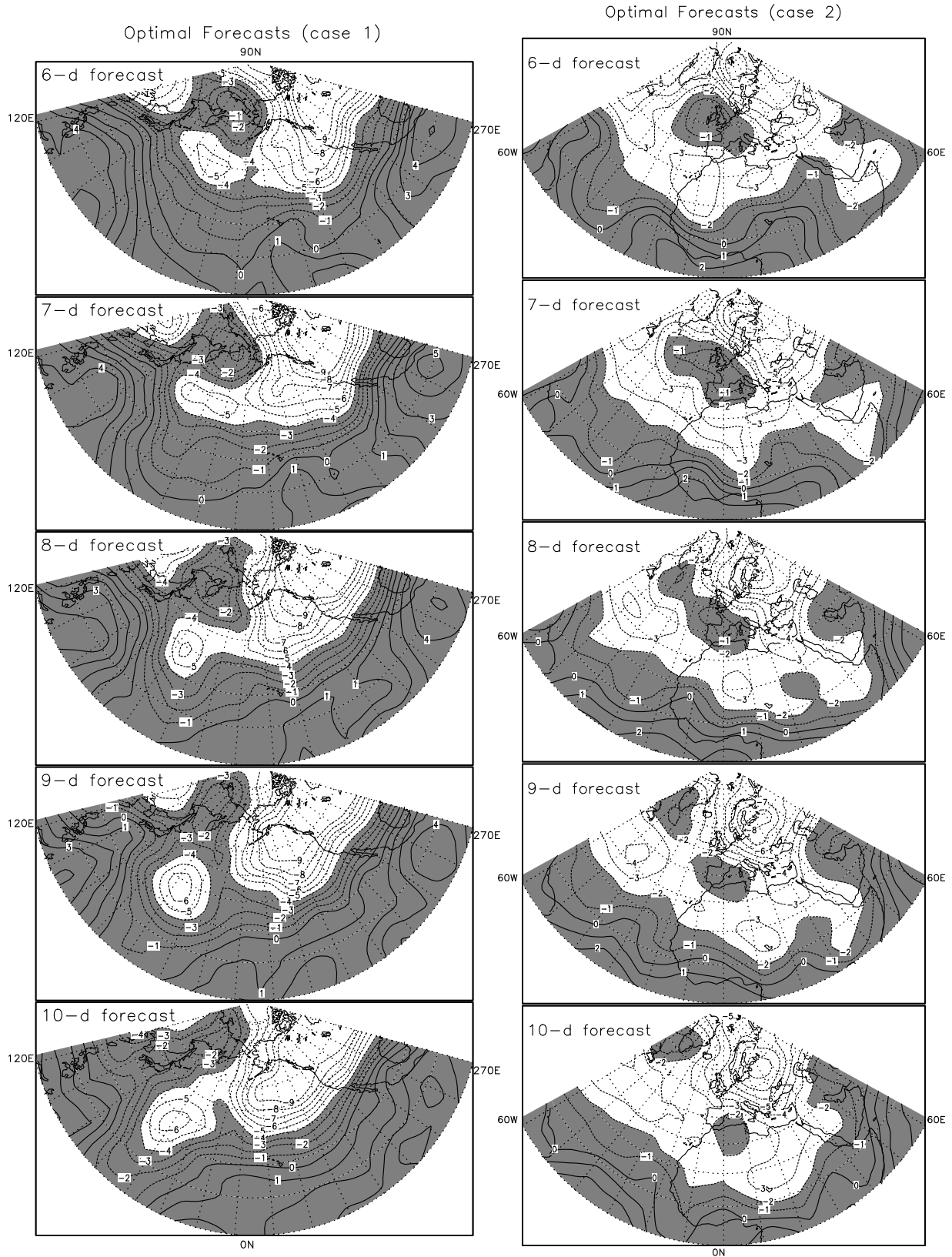


Figure 10: Same as Fig. 8, except for the optimal forecasts from day 6 to day 10 using the analysis streamfunctions at 00 UTC 28 December 1990 over the domain of 0-90°N, 120°E-270°E (left) and 00 UTC 1 November 1980 over the domain of 0-90°N, 60°W-60°E (right) as initial conditions, and that the shaded represents areas greater than  $-4 \times 10^7 m^2 s^{-1}$  (left) and  $-2 \times 10^7 m^2 s^{-1}$  (right).